RESPONSE OF THE IONOSPHERIC *F*2 LAYER TO THE GEOMAGNETIC STORM OF FEBRUARY 26–28, 2023

S.A. Riabova[1*]

[1] *Sadovsky Institute of Geosphere Dynamics of Russian Academy of Sciences, Moscow, Russia*

**e-mail: riabovasa@mail.ru*

Received March 18, 2024
Revised September 30, 2024
Accepted December 12, 2025

The results of research on the behavior of the main characteristics of the *F* -region of the ionosphere during the strong prolonged magnetic storm of February 26–28, 2023 are presented. The variations of the critical frequency of the *F* 2-layer of the ionosphere *foF* 2 (characterizing the maximum electron density) and the height of the maximum of the *F* 2-layer of the ionosphere *hmF* 2 are analyzed by their relative deviations from values under quiet conditions. In the European region, a positive pre-storm disturbance in *foF* 2 variations and a negative disturbance after the onset of the magnetic storm are identified. It is established that during the magnetic storm, the height *hmF* 2 changes significantly. The dependence of the ionospheric response on the location of the ionospheric station is shown.

Keywords: ionosphere, variation, critical frequency of the F2-layer, height of the F2-layer maximum, magnetic storm

DOI: 10.31857/S00167940250307e4

1. INTRODUCTION

Many aspects of the ionospheric effect of geomagnetic storms remain unclear, as the response of the *F* -region of the ionosphere to a magnetic storm is the result of many interconnected processes occurring in the magnetosphere, ionosphere, and upper atmosphere of the Earth [Danilov and Lastovička, 2001; Rishbeth, 1991]. It should be added that changes in the characteristics of the *F* -region during a storm occur over a wide altitude range (200-1000 km) [Blagoveshchenskiy, 2013; Grandin et al., 2015; Laštovička, 1996], and the ionospheric response to a specific storm largely depends on the sequence and intensity of various factors during the development of a particular geomagnetic disturbance [Romanova et al., 2013; Chernigovskaya et al., 2020, 2021; Bojilova and Mukhtarov, 2023]. During geomagnetic disturbances, the critical frequency of the *F* 2-layer of the

ionosphere may decrease or increase compared to values under quiet conditions (negative or positive ionospheric storms, respectively) [Matsushita, 1959]. Disturbed electric fields generated during magnetic storms (almost instantaneously appearing zonal electric fields of rapid penetration, often observed at equatorial latitudes, and delayed electric fields created by the disturbed dynamo as a result of Joule heating due to energy input during a magnetic storm at high latitudes) can cause large upward or downward flows of ionospheric plasma, leading to large-scale increases or decreases in electron concentration and vertical total electron content [Huang, 2013; Tsurutani et al., 2004]. The development of negative and positive effects of ionospheric storms strongly depends on local time, season, and geographic region [Buonsanto, 1999; Mendillo, 2006; Rishbeth, 1998]. It should be noted that magnetic storms cause an intensification of the ionospheric electric field, which leads to variations in the gradient of the electric field potential at the Earth's surface [Apsen et al., 1988]. The influence of magnetic storms on the atmospheric electric field has been studied in most works under auroral and subpolar latitude conditions, where the effect is more pronounced [for example, Frank-Kamenetsky et al., 2001; Frank-Kamenetskii et al., 2012; Kleimenova et al., 2012], while studies describing this effect for mid-latitude conditions are few [Anisimov et al., 2021; Kleimenova et al., 2008; Ryabova, 2020; Ryabova and Spivak, 2021].

Studies of ionospheric storms, including the effects of disturbances in the *F* -region, are very important from a practical point of view, since ionospheric disturbances directly affect satellite orbital characteristics, lead to errors in the global positioning system and navigation systems, and cause HF radio communication disruptions [Zakharov et al., 2016; Spivak et al., 2021; Astafyeva et al., 2022].

In connection with the above, conducting an analysis of the ionospheric response using various measurement tools and methods during magnetic storms is of significant scientific and practical interest. In this context, ionograms obtained during vertical sounding of the ionosphere are quite informative tools.

This work is devoted to the analysis of the ionospheric response to one of the strongest magnetic storms of 2023. During the research, relative variations of the critical frequency of the *F* 2-layer of the ionosphere *foF* 2 and the height of the maximum of the *F* 2-layer of the ionosphere *hmF* 2 during the strong magnetic storm of February 26-28, 2023, were studied in comparison with variations of ionospheric parameters under quiet conditions.

2. MAGNETIC STORM OF FEBRUARY 26-28, 2023

Solar activity during the period from February 26 to 28 was at a moderate level, with the *F* 10.7 index varying in the range of 156-158 sfu [SDO, 2023]. The magnetic storm began on February 26 at approximately 19:20-19:40 UT, continued throughout the day on February 27, and ended on February 28 at 3:00 UT. Within an hour after the arrival of coronal mass ejections, the level of the magnetic storm rapidly changed from G1 (minor) to G2 (moderate). The peak of the magnetic storm occurred on February 27 from 9:00 to 12:00 UT, with the *G* -index at this time reaching three out of five possible (G3), which is classified as a strong magnetic storm. The strong and prolonged magnetic storm caused auroras, which were observed in northern cities of Russia, in Belarus, Canada, northern Europe (as far south as Germany), as well as in the northern states of the USA.

Geomagnetic activity during the storm period was caused by a combination of two consecutive coronal mass ejections (CMEs) and high-speed streams from background coronal holes [SDO, 2023]. The first coronal mass ejection, containing a geoeffective component, was associated with the M3.7/2B solar flare on February 24 (maximum time - 20:30 UT, duration - 86 min, coordinates - N28W28 (active region 3229)). This flare was accompanied by radio emission bursts of spectral types II and IV. On February 24, the flare caused an intrusion of proton fluxes in a wide energy range into near-Earth space (NES). On February 25, another M6.3/3N class flare occurred in the same region with the following characteristics: maximum time - 19:44 UTC, duration - 107 min, coordinates - N26W43. The flare was accompanied by radio emission bursts of spectral types II and IV and a coronal mass ejection (partial halo-coronal mass ejection) containing a geoeffective component. On February 25-26, an intrusion of proton fluxes in a wide energy range into NES was recorded from the flare. The accelerated proton fluxes from the second flare were significantly stronger than the proton fluxes from the first flare.

In addition, from 19:49 to 20:16 UTC on February 24, 2023, in the region N19W34, a solar filament eruption was recorded, accompanied by a coronal mass ejection in the southwest direction (angle 76°, max speed 801 km/s). It should also be noted that on February 24-25, a medium-contrast coronal hole of negative polarity was located in the southern hemisphere and crossed the central meridian [SDO, 2023].

Fig. 1.

Analysis of solar wind parameters measured by the ACE spacecraft [NOAA, 2023] (Fig. 1) showed that at 18:50 UT on February 26, a heterogeneous accelerated flow from two coronal mass ejections (2 CMEs from February 24) arrived, with a proton concentration of 33 particles/cm ^{3}, the solar wind speed began to increase from ~ 450 km/s and by the end of February 26 reached 770 km/s. In the period from 19:30 to 22:30 UT on February 26, there was a three-hour southward turn

of the *Bz component* of the interplanetary magnetic field (IMF), fluctuations of the *Bz* -component of the IMF reached -19 nT. From the beginning of the day until 10 UT on February 27, a decrease in the solar wind speed to 600 km/s was observed, the value of the southern component of the IMF fluctuated from -13 to 8 nT. At 10 UT on February 27, a heterogeneous accelerated flow from a coronal hole and coronal mass ejection (CME from February 25) arrived, the solar wind speed began to increase and by 12 UT on February 27 reached a maximum value of 880 km/s. The *Bz* -component of the IMF was quite unstable and had a southern orientation for a fairly long time (07:00-12:30 UT) with a minimum value of -19 nT at 10:30 UT on February 27. Then the solar wind speed began to decrease and by 17 UT on February 28 reached a value of 550 km/s. As can be seen from Fig. 1, in the period from February 26 to 28, 2023, the change in the *SYM-H* index [ISGI, 2023] demonstrated several complex decreases following variations in the solar wind and the *Bz* -component of the IMF, ultimately reaching a minimum value of -161 nT at 12:10 UT on February 27 with a further gradual recovery of values on February 28. At 20 UT on February 26, the *Kp* index becomes equal to 5, *Dst* is about -40 nT [ISGI, 2023]. *Kp* exceeds 5 between 20 UT on February 26 and 2 UT on February 28. The maximum of the storm can be considered to be around noon on February 27. The three-hour geomagnetic index *Kp* had a value of 7 for 9 hours. Around 12 UT, the *Kp* index exceeded 6, the *Dst* index was between -130 and -140 nT, *SYM-H* reached its minimum value (-161 nT) at 12:10 UT, which corresponds to a strong (i.e., intense) disturbance. Then the recovery phase began.

3. INITIAL DATA AND METHODS

As initial data, vertical ionospheric sounding data published on the Global Ionospheric Radio Observatory website [GIRO, 2023] were used. In the present study, the ionospheric response was examined in the European region, with the list of ionospheric stations and their coordinates provided in Table 1, and their locations shown in Fig. 2. Based on ionogram data, the main ionospheric characteristics were determined, which were used to analyze the ionospheric response to the magnetic storm: hourly average values of the critical frequency *F* 2-layer of the ionosphere (f o F 2) and the height of the maximum of the *F* 2-layer of the ionosphere (*hmF* 2) through manual processing of ionograms with interpretation according to the URSI methodology [Manual..., 1977]. It should be noted that errors may occur during automatic determination of ionospheric parameters from ionograms, and regarding the critical frequency of the *F* 2-layer, several studies (see, for example, [Jiang et al., 2013]) have demonstrated that inaccuracies in determining values can reach 1-5 MHz. As an example, Fig. 3 shows variations in the critical frequency and the height of the

maximum of the *F* 2-layer of the ionosphere for the period from February 26 to 28, 2023, as well as averaged daily variations of these ionospheric parameters during a magnetically quiet period (five most magnetically quiet days according to [ISGI, 2023]) at the Moscow ionospheric station.

Table 1

Fig. 2.

Fig. 3.

During this study, a standard procedure was applied for filtering daily, seasonal behavior, as well as long-term fluctuations in solar activity, which affect the parameter values of the *F* 2-layer of the ionosphere, using the following formulas [Kumar and Kumar, 2022]:

$$\Delta f_o F_2 = (f_o F_2 - f_o F_{2\,mean}) / f_o F_{2\,mean},$$

$$\Delta hmF_2 = (hmF_2 - hmF_{2\,mean}) / hmF_{2\,mean},$$

where $f_o F_2$ – hourly average value of the critical frequency of the *F* 2-layer of the ionosphere, hmF_2 – hourly average value of the maximum height of the *F* 2-layer of the ionosphere during the magnetic storm period, $foF_{2\,mean}$ and $hmF_{2\,mean}$ – median hourly average values for February (for the five most magnetically quiet days according to [ISGI, 2023]) of the critical frequency and maximum height of the *F* 2-layer of the ionosphere, respectively.

4. RESULTS AND DISCUSSION

Data processing and analysis of vertical ionospheric sounding showed that at all ionospheric stations before and immediately after the onset of the magnetic storm, generally similar behavior of variations in the critical frequency *F* 2-layer of the ionosphere foF_2 is observed. Before the onset of the magnetic storm, an increase in relative values of foF_2 is observed, and immediately after its onset, the relative values of the critical frequency of the *F* 2-layer begin to decrease. As an example, Fig. 4 shows variations in the critical frequency of the *F* 2-layer of the ionosphere relative to background values at several European ionospheric stations: Warsaw, Gibilmanna, Dourbes, El Arenosillo, Moscow, Rome, Chilton, and Juliusruh. As can be seen from Fig. 4, at all stations, a positive bay is observed in the variations of relative values of foF_2 between 15 and 19 UT on February 26. Before the onset of the magnetic storm, a clear increase in relative values of critical frequency (ΔfoF_2) is noted. Maximum values of ΔfoF_2 at all ionospheric stations are observed at the moment of the magnetic storm onset and amount to: 29% at Warsaw station, 19% at Gibilmanna station, 17% at Dourbes station, 8% at El Arenosillo station, 32% at Moscow station, 8% at Rome station, 22% at Chilton station, and 29% at Juliusruh station, while the amplitude of variations was 24% at Warsaw station, 13% at Gibilmanna station, 8% at Dourbes station, 7% at El Arenosillo

station, 39% at Moscow station, 13% at Rome station, 22% at Chilton station, and 30% at Juliusruh station. The pre-storm increase was maximum in northern Europe, and the minimum pre-storm effect was observed at the station located in southwestern Europe. It should be noted that the pre-storm increase in *foF* 2 in the European region was also observed during three strong winter geomagnetic storms that occurred in January 2005 [Bojilova and Mukhtarov, 2019]. The positive disturbance in the variations of the critical frequency of the *F* 2-layer of the ionosphere, which is quite frequently observed before the onset of a geomagnetic storm and which was also detected at all ionospheric stations during the present research, is considered a manifestation of the pre-storm deviation phenomenon (ionospheric precursor) (for example, [Konstantinova and Danilov, 2019]). However, such precursors are still the subject of extensive discussion [Burešová and Laštovička, 2007]. Another reason why a positive response in *foF* 2 may occur before a magnetic storm could be unrelated to the magnetic storm; in this case, the ionospheric response is due to internal atmospheric processes [Mikhailov and Perrone, 2021]. According to this concept, such disturbances are manifestations of ionospheric perturbations that are occasionally observed under magnetically quiet conditions and can randomly occur on pre-storm days, although they have no relation to the upcoming storm.

Fig. 4.

The study of variations in the height of *hmF* 2 (height of the maximum of the *F* 2-layer of the ionosphere) relative to background levels showed that, in general, variations in the height of the maximum of the *F* 2-layer have a character opposite to changes in the critical frequencies of the *F* 2-layer, with significant height variations observed during nighttime. Figure 5 shows the variations in the height of *hmF* 2 relative to background levels (Δ *hmF* 2) at several European ionospheric stations: Athens, Dourbes, El Arenosillo, Nicosia, Moscow, San Vito, Chilton, and Juliusruh. As can be seen from Figure 5, the behavior of Δ *hmF* 2 variations differs slightly at different ionospheric stations. At Dourbes and Chilton stations (Fig. 5), a response in Δ *hmF* 2 in the form of a positive bay is recorded before the onset of the magnetic storm and approximately until 20 UT.

Fig. 5.

At all stations after the onset of the magnetic storm, a sharp decrease in Δ *foF* 2 and an almost simultaneous increase in Δ *hmF* 2 are observed, and at 20 UT a sharp decrease in relative values of height *hmF* 2 is noted. It should be noted here that the strongest negative response is observed at ionospheric stations located in the southeastern part of Europe. As can be seen from Fig. 5, at Nicosia and Athens stations at 20 UT, Δ *hmF* 2 reaches a value of approximately - 15%. At stations located in the northern part of Europe (Moscow, Fairford, Chilton, and Juliusruh), a very

weak negative response is also visible at approximately 20 UT, with Δ *hmF* 2 values approaching 0% (Fig. 5). Processing and analysis of vertical sounding results demonstrated that the negative response of Δ *hmF* 2 at northern stations is much weaker than at stations located at lower latitudes, which can be explained by effects associated with the restructuring of the equatorial anomaly of the *F* 2-layer of the ionosphere. The data in Fig. 4 indicate that in the period from 20 UT on February 26 to 05 UT on February 27 (in nighttime conditions), a bay-shaped decrease in Δ *foF* 2 is observed at middle latitudes. The minimum values of Δ *foF* 2 are: - 35% at Warsaw station, - 25% at Gibilmanna station, - 22% at Dourbes station, - 23% at El Arenosillo station, - 29% at Moscow station, - 11% at Rome station, - 33% at Chilton station, and - 30% at Juliusruh station. Attention should be paid to the fact that the negative disturbance of *foF* 2 occurs almost without delay after the onset of the magnetic storm, and this pattern is observed down to low latitudes (Nicosia and Athens stations). The height of the maximum of the *F* 2-layer on the night of February 26-27 increases after 21 UT, which is a typical reaction of the nighttime ionosphere during a magnetic storm at middle latitudes [Gordienko et al., 2011]. Between midnight and 08 UT on February 27, fluctuations of Δ *hmF* 2 are recorded at all ionospheric stations considered in this paper, which were most pronounced at stations in the southeast of Europe. Statistical generalization and detailed examination of the total electron content response to geomagnetic disturbances in winter conditions [Andonov et al., 2021] show the appearance of a negative anomaly region at middle latitudes south of the positive anomaly region at auroral latitudes during post-midnight hours in local time. The nighttime decrease in Δ *foF* 2 in the European segment was probably caused by the movement of the mid-latitude ionospheric trough toward lower latitudes [Matyjasiak et al., 2016]. The analysis of total electron content maps over the European region shows a displacement of the ionospheric trough toward low latitudes. Also, the nighttime decrease in Δ *foF* 2 may be caused by partial depletion of the plasmasphere, which leads to a decrease in the downward flux of H+ ions, which is responsible for increasing the electron concentration of the *F* 2-layer at middle latitudes during winter nights [Kotov et al., 2016, 2018]. The cause of such a response may be disturbances in the lower thermosphere caused by gas heating by auroral electrojets [Shpynev et al., 2017]. It is known that this heating causes an increase in neutral wind velocity and intensification of turbulence in the lower ionosphere. This, in turn, leads to a decrease in the $[O]/[N_2]$ ratio at upper atmosphere heights and, accordingly, an increase in recombination, which, in the absence of ionizing radiation, causes a significant decrease in electron density [Mayr and Volland, 1972; Laštovička, 2002; Prölss and Werner, 2002; Danilov, 2003; Liou et al., 2005; Kil et al., 2011; Klimenko et al., 2011]. Enhanced recombination due to increased molecular nitrogen density is unlikely to be the cause of the decrease, as insufficient time has passed

since the beginning of the storm. The influence of electric fields created by anomalous dynamics of the neutral atmosphere during a magnetic storm may also form the ionospheric response [Kelley et al., 2004].

Moderate positive ionospheric storm was observed during the main phase of the magnetic storm on February 27 during the daytime. Several hours before and around noon, the response of $foF2$ (Fig. 4) becomes positive, and the response of $hmF2$ becomes negative, which is the result of the expansion of the equatorial ionization anomaly towards middle latitudes under the influence of the disturbed component of the meridional wind, which at low latitudes is deflected in the zonal direction due to the Coriolis acceleration [Heelis et al., 2009]. The magnetic storm of February 26-28 reaches its maximum around noon on February 27, when daytime conditions prevail in the European region. At 12 UT, $\Delta foF2$ is 20% at Warsaw station, 14% at Gibilmanna station, 7% at Dourbes station, 1% at El Arenosillo station, 1% at Moscow station, 14% at Rome station, 1% at Chilton station, and 15% at Juliusruh station. During the main phase of the magnetic storm, a decrease in $\Delta hmF2$ values down to 0% is observed. Analysis of neutral composition measurements using the GUVI TIMED UV spectrometer at lower thermosphere altitudes (~100 km) showed that during the magnetic storm, a region of elevated [O]/[N_2 values was located over the European region.

After 16 UT, the process of negative anomaly propagation from north to south begins, which is the result of heated air transfer; this corresponds to the total electron content distribution maps. The decrease in electron density compensates for the increase caused by the expansion of the equatorial ionospheric anomaly. The shift toward low latitudes of the ionospheric trough during nighttime hours is clearly manifested on the total electron content maps over the European region. According to data from European ionospheric stations, a latitudinal dependence is observed for negative disturbances of the relative values of the critical frequency (Fig. 4). The strongest response is observed at northern stations (Warsaw, Fairford, Chilton, Moscow, and Juliusruh). $\Delta foF2$ is less than −38% at Warsaw station, −54% at Moscow station, −59% at Chilton station, and −61% at Fairford station. At southern stations (Athens, Gibilmanna, Nicosia, Rome, and San Vito), the negative response is weak, and it even turns positive after 20 UT on February 27. $\Delta foF2$ is 1% at Athens, 8% at Gibilmanna, 3% at Nicosia, −6% at Rome, and −4% at San Vito. In the variations of relative values of $hmF2$ (Fig. 5), a sharp increase in the height of the $F2$-layer maximum is observed around 18 UT on February 27 and around 02 UT on February 28, with this increase being stronger in Eastern Europe and weaker in Western Europe.

5. CONCLUSION

In the course of the present research, variations in the critical frequency *foF* 2 and the height of the maximum (*hmF* 2) of the ionospheric *F* 2-layer before the onset of the magnetic storm on February 26–28, 2023, and during its development were analyzed. During the processing of data from fourteen ionospheric stations in the European region, disturbances in *foF* 2 variations were identified: positive pre-storm and negative after the onset of the magnetic storm. During the development of the magnetic storm, a significant change in the height of *hmF* 2 was noted. In general, the response of ionospheric parameters depends on the location of the ionospheric station, which is consistent with the results of previous studies (for example, [Romanova, 2013; Chernigovskaya et al., 2020].

According to the author, the data obtained in this work supplement the currently existing understanding of the ionospheric response to strong magnetic storms and may prove useful in a comprehensive description of the effects of magnetic storms, improving existing and developing new models of these phenomena important for the habitat, including the assessment of the main ionospheric trough, the construction of an empirical model of which remains a complex task today, since the position of the ionospheric trough depends on local time, longitude, solar and magnetic activity [Namgaladze et al., 1990; Deminov and Shubin, 2018].

FUNDING

The research was carried out within the framework of the State Assignment of IDG RAS No. 122032900185-5 "Manifestation of processes of natural and technogenic origin in geophysical fields".

REFERENCES

− *Anisimov S.V., Shikhova N.M., Kleimenova N.G.* Response of the magnetospheric storm in the atmospheric electric field of middle latitudes // Geomagnetism and Aeronomy. Vol. 61. No. 2. P. 172–183. 2021. https://doi.org/10.31857/S0016794021020024

−*Apsen A.G., Kanonidi Kh.D., Chernysheva S.P., Sheftel V.M.* Magnetospheric effects in atmospheric electricity. Moscow: Nauka, 150 p. 1988.

−*Blagoveshchensky D.V.* The influence of geomagnetic storms/substorms on the ionosphere. Part 1. (Review) // Geomagnetism and Aeronomy. Vol. 53. No. 3. P. 291–307. 2013. https://doi.org/10.7868/S0016794013030036

−*Deminov M.G., Shubin V.N.* Empirical model of the position of the main ionospheric trough // Geomagnetism and Aeronomy. Vol. 58. No. 3. P. 366–373. 2018. https://doi.org/10.7868/S0016794018030070

−*Zakharov V.I., Yasyukevich Yu.V., Titova M.A.* The influence of magnetic storms and substorms on GPS navigation system failures at high latitudes // Cosmic Research. Vol. 54. No. 1. P. 23–33. 2016. https://doi.org/10.7868/S0023420616010143

−*Kleimenova N.G., Kozyreva O.V., Kubicki M., Odzimek A., Malysheva L.M.* Influence of substorms in the Earth's night sector on variations of the surface atmospheric electric field in polar and equatorial latitudes // Geomagnetism and Aeronomy. Vol. 52. No. 4. P. 494–500. 2012.

−*Kleimenova N.G., Kozyreva O.V., Michnowski S., Kubicki M.* Effect of magnetic storms on variations of the atmospheric electric field at middle latitudes // Geomagnetism and Aeronomy. Vol. 48. No. 5. P. 650–659. 2008.

−*Konstantinova A.V., Danilov A.D* . Behavior of the ionospheric F *F* 2 region before a geomagnetic storm // Heliogeophys. research. Vol. 22. P. 33–51. 2019.

−*Namgaladze A.A., Korenkov Yu.N., Klimenko V.V., Karpov I.V., Bessarab F.S., Surotkin V.A., Glushchenko T.A., Naumova N.M.* Global numerical model of the Earth's thermosphere, ionosphere and protonosphere // Geomagnetism and Aeronomy. Vol. 30. No. 4. P. 612–619. 1990.

−*Romanova E.B., Zherebtsov G.A., Ratovsky K.G., Polekh N.M., Shi D., Wang S., Wang G.* Comparison of the F *F* 2-region ionosphere response to geomagnetic storms at middle and low latitudes // Solar-Terrestrial Physics. Vol. 22. P. 27–30. 2013.

− URSI Handbook on Ionogram Interpretation and Processing. Ed. N.V. Mednikova. Moscow: Nauka, 342 p. 1977.

− *Ryabova S.A.* Investigation of variations in electric field parameters during magnetic storms in 2018 // Processes in Geospheres. No. 4(26). P. 948–956. 2020.

−*Ryabova S.A., Spivak A.A* . Variations in electrical characteristics of the near-surface atmosphere during magnetic storms // Doklady Earth Sciences. Vol. 497. No. 1. P. 71−77. 2021. https://doi.org/10.31857/S2686739721030099

−*Spivak A.A., Ryabova S.A., Rybnov Yu.S., Kharlamov V.A* . GPS positioning errors during magnetic storms // Doklady Earth Sciences. Vol. 500. No. 2. P. 173–177. 2021. https://doi.org/10.31857/S2686739721100169

−*Chernigovskaya M.A., Shpynev B.G., Yasyukevich A.S.* et al. Longitudinal variations in the response of the mid-latitude ionosphere of the northern hemisphere to the geomagnetic storm in October 2016 using multi-instrumental observations // Current problems in remote sensing of the Earth from space. Vol. 18. No. 5. P. 305–317. 2021. https://doi.org/10.21046/2070-7401-2021-18-5-305-317

−*Chernigovskaya M.A., Shpynev B.G., Yasyukevich A.S., Khabituev D.S* . Ionospheric longitudinal variability in the northern hemisphere during magnetic storms according to ionosonde and GPS/GLONASS data // Current problems in remote sensing of the Earth from space. Vol. 17. No. 4. P. 269–281. 2020. https://doi.org/10.21046/2070-7401-2020-17-4-269-281.

−*Shpynev B.G., Zolotukhina N.A., Polekh N.M. et al.* Study of the ionospheric response to a strong geomagnetic storm in March 2015 based on data from the Eurasian chain of ionosondes //Modern problems of remote sensing of the Earth from space. Vol. 14. No. 4. P. 235–248. 2017. https://doi.org/10.21046/2070-7401-2017-14-4-235-248

−*Andonov B., Bojilova R., Mukhtarov P.* Global distribution of total electron content response to weak geomagnetic activity // Comptes rendus de l'Acade'mie bulgare des Sciences. V. 74. № 7. P. 1032–1042. 2021. https://doi.org/10.7546/CRABS.2021.07.10

−*Astafyeva E., Yasyukevich Y.V., Maletckii B., Oinats A., Vesnin A., Yasyukevich A.S., Syrovatskii S., Guendouz N* . Ionospheric disturbances and irregularities during the 25–26 August 2018 geomagnetic storm // J. Geophys. Res.− Space. V. 127. № 1. ID e2021JA029843. 2022. https://doi.org/10.1029/2021JA029843

−*Bojilova R., Mukhtarov P* . Comparative analysis of global and regional ionospheric responses during two geomagnetic storms on 3 and 4 February 2022 // Remote Sensing. V. 15. № 7. ID 1739. 2023. https://doi.org/10.3390/rs15071739

−*Bojilova R., Mukhtarov P* . Response of the electron density profiles to geomagnetic disturbances in January 2005 // Stud. Geophys. Geod. V. 63. № 3. P. 436–454. 2019. https://doi.org/10.1007/s11200-019-0510-6

−*Buonsanto M.J.* Ionospheric storms − a review // Space Sci. Rev. V. 88. № 3–4. P. 563–601. 1999. https://doi.org/10.1023/A:1005107532631

−*Burešová D., Laštovička J.* Pre-storm enhancements of *foF* 2 above Europe // Adv. Space Res. V. 39. № 8. P. 1298–1303. 2007. https://doi.org/10.1016/j.asr.2007.03.003

−*Danilov A.D.* Long-term trends of *foF* 2 independent on geomagnetic activity // Ann. Geophys. V. 21. № 5. P. 1167–1176. 2003. https://doi.org/10.5194/angeo-21-1167-2003

−*Danilov A.D., Lastovička J.* Effects of geomagnetic storms on the ionosphere and atmosphere // International Journal of Geomagnetism and Aeronomy. V. 2. № 3. P. 209–224. 2001.

−*Frank-Kamenetskii A.V., Kotikov A.L., Kruglov A.A., Burns G.B., Kleimenova N.G., Kozyreva O.V., Kubitski M., Odzimek A.* Variations in the near-surface atmospheric electric field at high latitudes and ionospheric potential during geomagnetic perturbations // Geomagn. Aeronomy. V. 52. № 5. P. 629–638. 2012. https://doi.org/10.1134/S0016793212050064

−*Frank-Kamenetsky A.V., Trochichev O.A., Burns G.B., Papitashvili V.O.* Variations of the atmospheric electric field in the near-pole region related to the interplanetary magnetic field // J. Geophys. Res. – Space. V. 106. № 1. P. 179–190. 2001. https://doi.org/10.1029/2000JA900058

−*Gordienko G.I., Vodyannikov V.V., Yakovets A.F.* Geomagnetic storm effects in the ionospheric *E* - and *F* -regions // J. Atmos. Sol-Terr. Phy. V. 73. № 13. P. 1818–1830. 2011. https://doi.org/10.1016/j.jastp.2011.04.008

−*Grandin M., Aikio A.T., Kozlovsky A., Ulich T., Raita T* . Effects of solar wind high-speed streams on the high-latitude ionosphere: Superposed epoch study // J. Geophys. Res. – Space. V. 120. № 12. P. 10669–10687. 2015. https://doi.org/10.1002/2015JA021785

−*Heelis R.A., Sojka J.J., David M., Schunk R.W* . Storm time density enhancements in the middle-latitude dayside ionosphere // J. Geophys. Res. – Space. V. 114. № 3. ID A03315. 2009. https://doi.org/10.1029/2008JA013690

−*Huang C.M.* Disturbance dynamo electric fields in response to geomagnetic storms occurring at different universal times // J. Geophys. Res. – Space. V. 118. № 1. P. 496–501. 2013. https://doi.org/10.1029/2012JA018118

−*Jiang C., Yang G., Zhao Z., Zhang Y., Zhu P., Sun H* . An automatic scaling technique for obtaining *F* 2 parameters and *F* 1 critical frequency from vertical incidence ionograms // Radio Sci. V. 48. № 6. P. 739–751. 2013. https://doi.org/10.1002/2013RS005223

−*Kelley M.C., Vlasov M.N., Foster J.C., Coster A.J* . A quantitative explanation for the phenomenon known as storm-enhanced density // Geophys. Res. Lett. V. 31. № 19. ID L19809. 2004. https://doi.org/10.1029/2004GL020875

−*Kil H., Kwak Y.S., Paxton L.J., Meier R.R., Zhang Y.* O and N2 disturbances in the *F* region during the 20 November 2003 storm seen from TIMED/GUVI // J. Geophys. Res. – Space. V. 116. № 2. ID 02314. 2011. https://doi.org/10.1029/2010JA016227

−*Klimenko M.V., Klimenko V.V., Ratovsky K.G., Goncharenko L.P., Sahai Y., Fagundes P.R., de Jesus R., de Abreu A.J., Vesnin A.M.* Numerical modeling of ionospheric effects in the middle- and low-latitude *F* region during geomagnetic storm sequence of 9–14 September 2005 // Radio Sci. V. 46. № 3. ID RS0D03. 2011. https://doi.org/10.1029/2010RS004590

−*Kotov D.V., Richards P.G., Bogomaz O.V., Chernogor L.F., Truhlík V., Emelyanov L.Ya., Chepurnyy Ya.M., Domnin I.F.* The importance of neutral hydrogen for the maintenance of the midlatitude winter nighttime ionosphere: evidence from IS observations at Kharkiv, Ukraine, and field line interhemispheric plasma model simulations // J. Geophys. Res. – Space. 2016. V. 12. № 7. P. 7013–7025. https://doi.org/10.1002/2016JA022442

−*Kotov D.V., Richards P.G., Truhlík V. et al.* Coincident observations by the Kharkiv IS radar and ionosonde, DMSP and Arase (ERG) Satellites, and FLIP model simulations: implications for the NRLMSISE-00 hydrogen density, plasmasphere, and ionosphere // Geophys. Res. Lett. 2018. V. 45. № 16. P. 8062–8071. https://doi.org/10.1029/2018GL079206

−*Kumar E.A., Kumar S* . Geomagnetic storm effect on *F* 2-region ionosphere during 2012 at low- and mid-latitude stations in the Southern hemisphere // Atmosphere. V. 13. № 3. ID 480. 2022. https://doi.org/10.3390/atmos13030480

−*Laštovička J.* Effects of geomagnetic storms in the lower ionosphere, middle atmosphere and troposphere // J. Atmos. Terr. Phys. V. 58. № 7. P. 831 – 843 . 1996. https://doi.org/10.1016/0021-9169(95)00106-9

−*Laštovička J* . Monitoring and forecasting of ionospheric space weather effects of geomagnetic storms // J. Atmos. Sol.-Terr. Phy. V. 64. № 5–6. P. 697–705. 2002. https://doi.org/10.1016/S1364-6826(02)00031-7

−*Liou K., Newell P.T., Anderson B.J., Zanetti L., Meng C.-I* . Neutral composition effects on ionospheric storms at middle and low latitudes // J. Geophys. Res. – Space. V. 110. № 5. ID A05309. 2005. https://doi.org/10.1029/2004JA010840

−*Matsushita S* . A study of the morphology of ionospheric storms// J. Geophys. Res. V. 64. № 3. P. 305–321. 1959. https://doi.org/10.1029/JZ064i003p00305

−*Matyjasiak B., Przepiórka D., Rothkaehl H* . Seasonal variations of mid-latitude ionospheric trough structure observed with DEMETER and COSMIC // Acta Geophys. 2016. V. 64. № 6. P. 2734–2747. https://doi.org/10.1515/acgeo-2016-0102

−*Mayr H.G., Volland H* . Magnetic storm effects in the neutral composition // Planet. Space Sci. V. 20. № 3. P. 379–393. 1972. https://doi.org/10.1016/0032-0633(72)90036-0

−*Mendillo M.* Storms in the ionosphere: Patterns and processes for total electron content // Rev. Geophys. V. 44. № 4. ID RG4001. 2006. https://doi.org/10.1029/2005RG000193

−*Mikhailov A.V., Perrone L* . Pre-storm *F* 2-layer Q-disturbances at middle latitudes: Do they exist? // J. Atmos. Sol.-Terr. Phy. V. 213. ID 105473. 2021. https://doi.org/10.1016/j.jastp.2020.105473

−*Prölss G.W., Werner S* . Vibrationally excited nitrogen and oxygen and the origin of negative ionospheric storms // J. Geophys. Res. – Space. V. 107. № 2. ID 1016. 2002. https://doi.org/10.1029/2001JA900126

−*Rishbeth H. F* -region storms and thermospheric dynamics // J. Geomag. Geoelectr. V. 43. Suppl. P. 513–524. 1991. https://doi.org/10.5636/jgg.43.Supplement1_513

−*Rishbeth H.* How the thermospheric circulation affects the ionospheric *F* 2-layer // J. Atmos. Sol.-Terr. Phy. V. 60. № 14. P. 1385–1402. 1998. https://doi.org/10.1016/S1364-6826(98)00062-5

−*Tsurutani B., Mannucci A., Iijima B. et al.* Global dayside ionospheric uplift and enhancement associated with interplanetary electric fields // J. Geophys. Res.− Space. V. 109. № 8. ID A08302. 2004. https://doi.org/10.1029/2003JA010342

ISGI (2023). International Service of Geomagnetic Indices. http://www.isgi.unistra.fr

NOAA (2023). ACE real-tıme solar wınd. https://www.swpc.noaa.gov/products/ace-real-time-solar-wind

SDO (2023). Solar Dynamics Observatory. https://sdo.gsfc.nasa.gov/

GIRO (2023). Global ionosphere radio observatory. https://giro.uml.edu/

Table 1. Data from ionospheric stations

Name	Code	GEO		Ionosonde type
		Latitude	Longitude	
Athens (Greece)	AT138	38.0	23.6	DPS-4D
Warsaw (Poland)	MZ152	52.2	21.1	VISRC2
Gibilmanna (Italy)	GM037	37.9	14	AIS-INGV
Dourbes (Belgium)	DB049	50.1	4.6	DPS-4D
Moscow (Russia)	MO155	55.47	37.3	DPS-4D
Nicosia (Cyprus)	NI135	35.0	33.2	DPS-4D
Pruhonice (Czech Republic)	PQ052	50.0	14.6	DPS-4D
Rome (Italy)	RM041	41.8	12.5	DPS-4
San Vito (Italy)	VT139	40.6	17.8	DPS-4D
Fairford (United Kingdom)	FF051	51.7	-1.5	DPS-4D
Chilton (United Kingdom)	RL052	51.5	-0.6	DPS-1
Sopron (Hungary)	SO148	47.7	16.1	DPS-4D
El Arenosillo (Spain)	EA036	37.1	-6.7	DPS-4D
Juliusruh (Germany)	JR055	54.6	13.4	DPS-4D

Figure captions

Fig. 1. Variations of solar wind parameters: *Bz component* of interplanetary magnetic field (*Bz* - IMF), solar wind velocity v_{sw} and proton concentration (solar wind density) and variations of geomagnetic planetary indices *Kp, Dst* and *SYM-H* .

Fig. 2. Map of ionospheric stations in the European region (station codes are shown in the figure field).

Fig. 3. Variations in critical frequency and height of the maximum *F* 2-layer of the ionosphere for the period from February 26 to 28, 2023 . (circles) and averaged daily variations of these ionospheric parameters during magnetically quiet period (solid line) at the Moscow ionospheric station; vertical line – the beginning of the magnetic storm.

Fig. 4. Variations in the critical frequency of the *F* 2-layer of the ionosphere relative to background values for the period February 26–28, 2023 at ionospheric stations: Warsaw, Gibilmanna, Dourbes, El Arenosillo, Moscow, Rome, Chilton and Juliusruh (station codes are given in the figure field); vertical line – the beginning of the magnetic storm.

Fig. 5. Variations in the height of the maximum of the *F* 2 layer of the ionosphere relative to background values at ionospheric stations: Athens, Dourbes, El Arenosillo, Nicosia, Moscow, San Vito, Chilton and Juliusruh (station codes are given in the figure field); vertical line – the beginning of the magnetic storm.

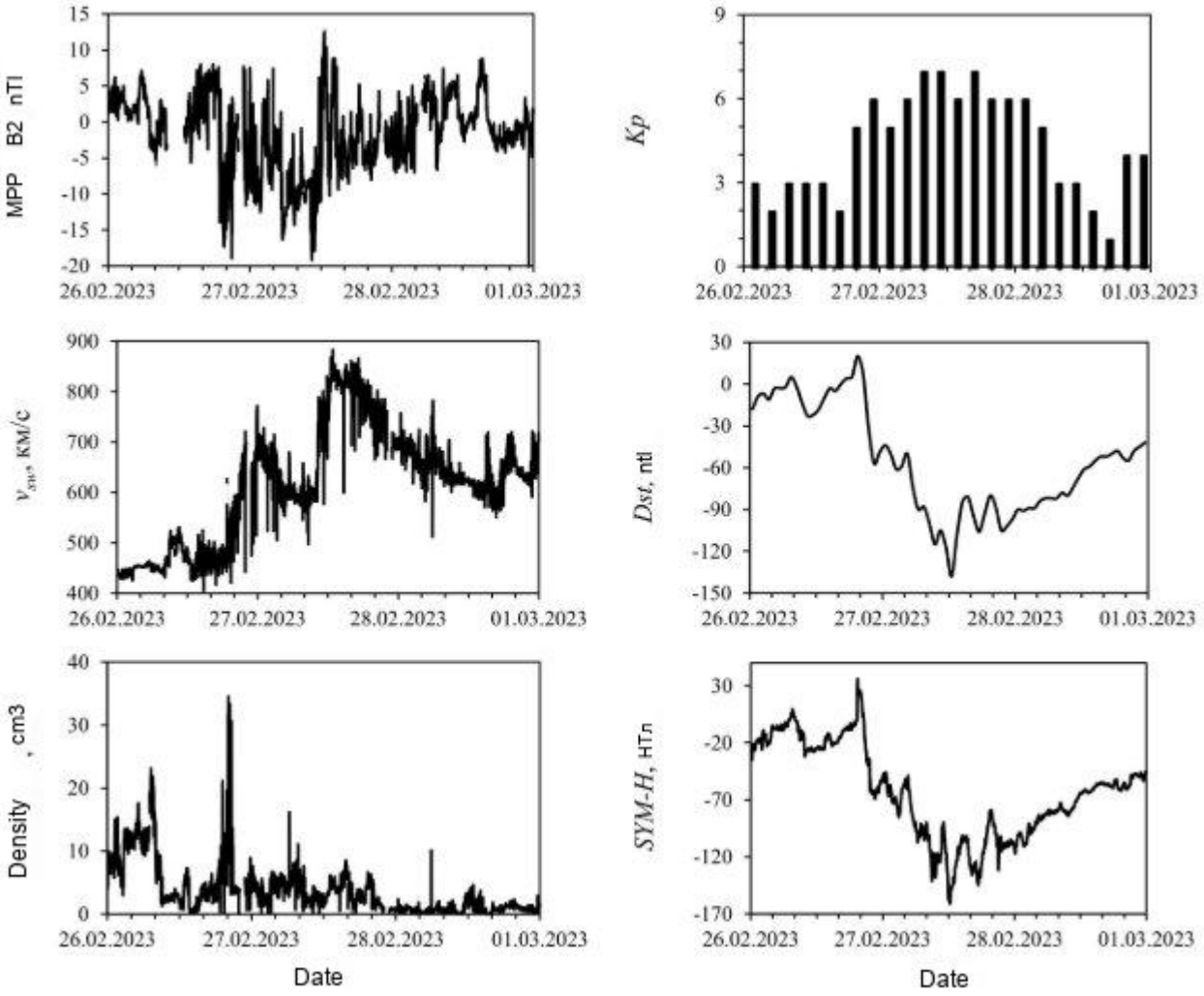
MPP B2 nTl
15
10
5
0
-5
-10
-15
-20
26.02.2023
27.02.2023
28.02.2023
01.03.2023
Kp
9
6
3
0
v_{sw}, KM/c
900
800
700
600
500
400
Dst, ntl
30
0
-30
-60
-90
-120
-150
Density , cm3
40
30
20
10
0
SYM-H, нТл
-20
-70
-120
-170
Date

Fig. 1.

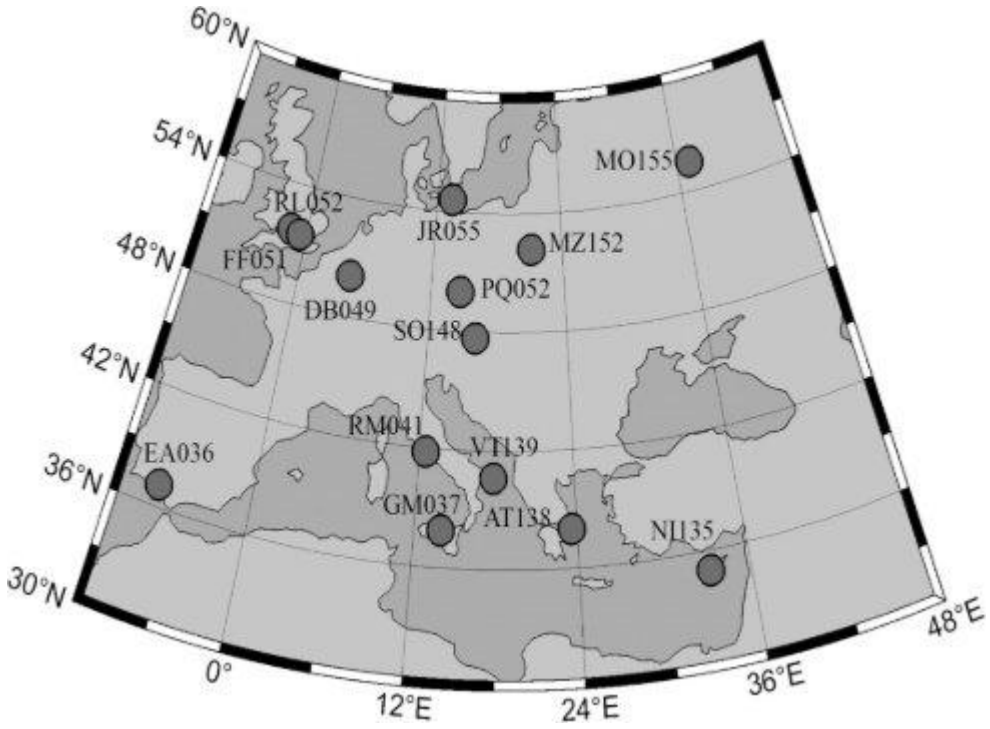
60°N
54°N
48°N
42°N
36°N
30°N
0°
12°E
24°E
36°E
48°E
MO155
RL052
JR055
MZ152
FF051
PQ052
DB049
SO148
RM041
VT139
EA036
GM037
AT138
NI135

Fig. 2.

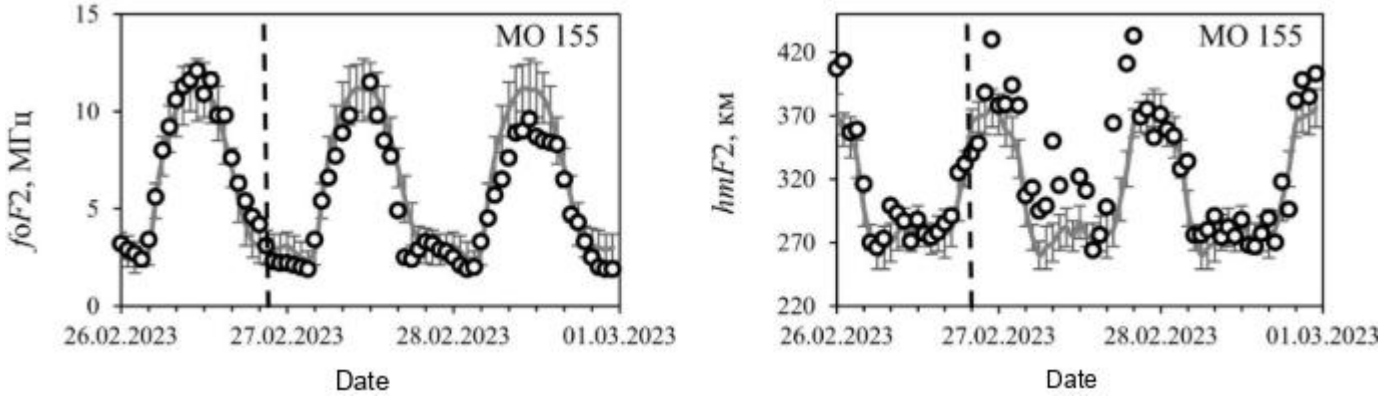
MO 155
foF2, МГц
15
10
5
0
26.02.2023
27.02.2023
28.02.2023
01.03.2023
Date
MO 155
hmF2, км
420
370
320
270
220
26.02.2023
27.02.2023
28.02.2023
01.03.2023
Date

Fig. 3.

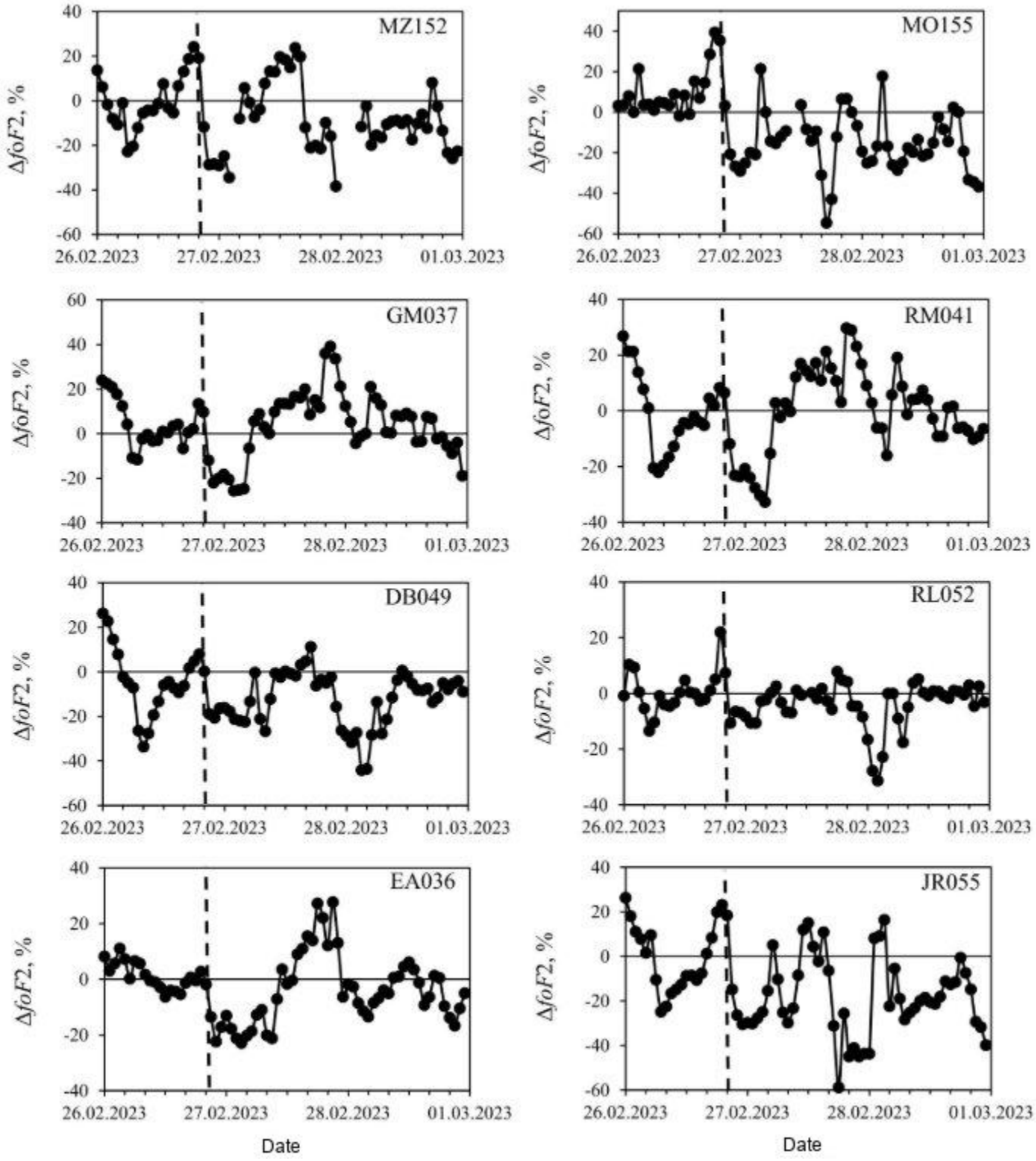
MZ152
MO155
GM037
RM041
DB049
RL052
EA036
JR055
ΔfoF2, %
40
20
0
-20
-40
-60
26.02.2023
27.02.2023
28.02.2023
01.03.2023
Date

Fig. 4.

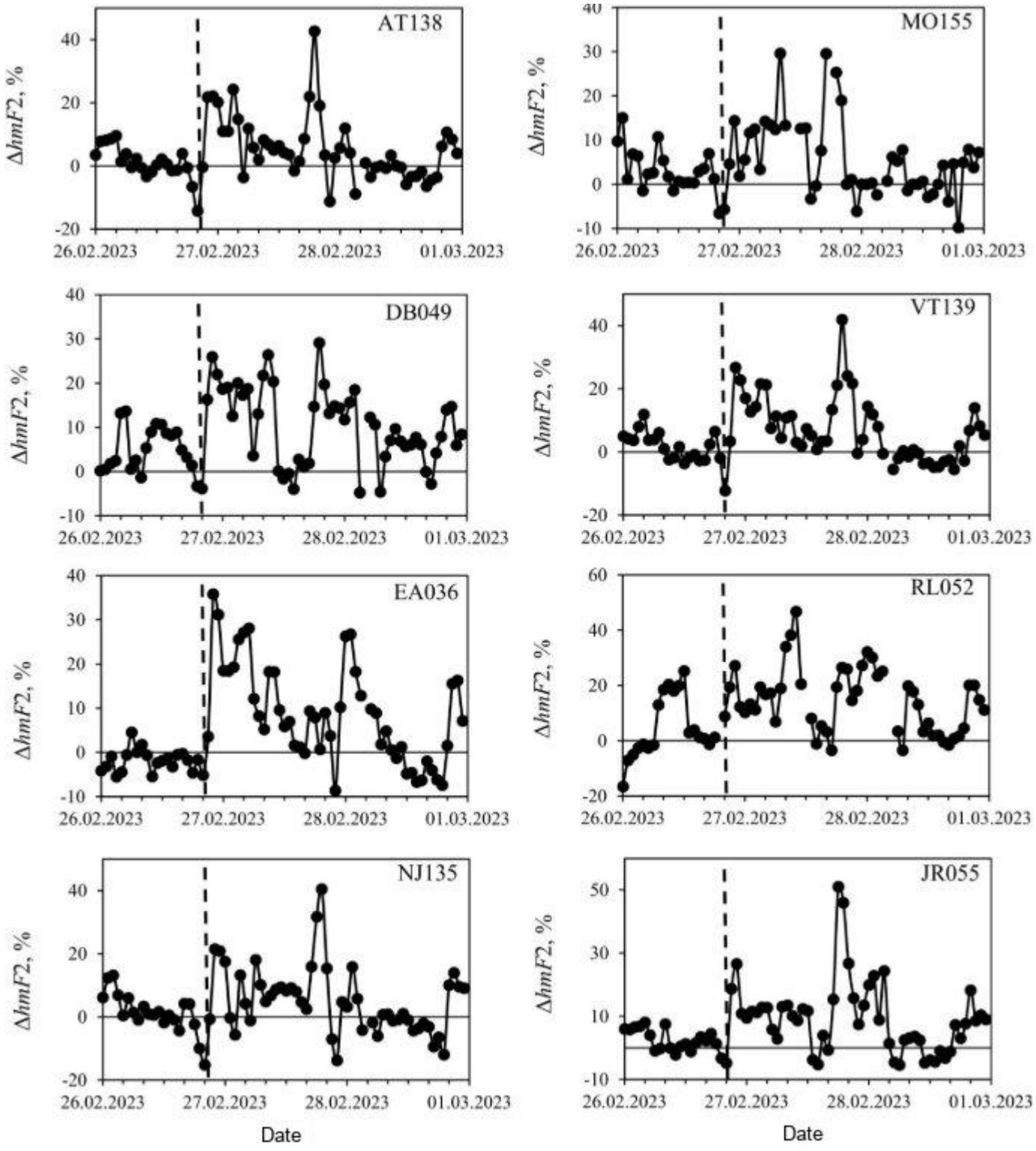
AT138
MO155
DB049
VT139
EA036
RL052
NJ135
JR055
ΔhmF2, %
26.02.2023
27.02.2023
28.02.2023
01.03.2023
Date

Fig. 5.